5-2019

# Design and Development of Hybrid Rocket for Spaceport America Cup

Benjamin Barnhill
*University of Tennessee-Knoxville*, bbarnhi2@vols.utk.edu

Sean Darling
*University of Tennessee-Knoxville*, sdarlin3@vols.utk.edu

Austin Springer
*University of Tennessee-Knoxville*, aspring5@vols.utk.edu

Adam Todd
*University of Tennessee-Knoxville*, atodd15@vols.utk.edu

Stewart Whaley
*University of Tennessee-Knoxville*, swhaley7@vols.utk.edu

# Design and Development of Hybrid Rocket for Spaceport America Cup

Benjamin Barnhill,[1] Sean Darling,[2] Austin Springer,[3] Adam Todd,[4] and Stewart Whaley[5]
*University of Tennessee Knoxville, Knoxville, TN, 37920, U.S.A.*

**The senior design team advised by Dr. Evans Lyne was tasked with creating a student researched and developed hybrid liquid engine capable of propelling an 8.8 pound payload to 10,000 ft. To accomplish this, the motor of a typical hybrid engine was modified to include a 3D-printed, coal-packed matrix fuel grain, a new nozzle with added post-combustion chamber, and dissociative catalysts to the solid fuel. The matrix fuel grain showed an increase of specific impulse from 27.1% to 52.4% when compared to standard grain types due to an increase in fuel regression rates. The added post-combustion chamber allowed the motor to achieve combustion efficiency of 86% of theoretical by increasing time for coal powder to ignite. The catalytic introduction to fuel showed a greater increase in nitrous dissociation when subject to less oxidizer flow, although further testing is needed to better quantify its benefits at operating conditions.**

## I. Nomenclature

| | | |
|---|---|---|
| $A_t$ | = | area of the throat of the nozzle |
| $C^*$ | = | characteristic velocity |
| $C_N$ | = | nozzle coefficient |
| $g_o$ | = | gravitational field constant |
| $I_{tot}$ | = | total impulse |
| $I_{sp}$ | = | specific impulse |
| $\dot{m}$ | = | mass flow |
| $m_{burned}$ | = | mass of propellant burned |
| $P$ | = | pressure |
| $T$ | = | thrust |
| $t_{burn}$ | = | burn time |

## II. Introduction

The Intercollegiate Rocketry Engineering Competition (IREC) is an international initiative which allows student rocketry teams to launch experimental payloads on student-designed motors to various altitudes. UT's competition team will attempt to launch an 8.8 pound payload to 10,000 feet to collect microbial samples from the upper atmosphere. The competition allows for teams to design motors of differing fuel types ranging from commercial off the shelf (COTS) to bi-propellant liquid engines. The motor category UT's competition team entered into was the Student Researched and Developed (SRAD) Hybrid Liquid Engine. Therefore, the senior design team advised by Dr. Evans Lyne, a researcher at UT whose work centers around hybrid motor development, was tasked with designing and creating a motor capable of fulfilling the design criteria.

To create a hybrid motor capable of carrying such a large payload to the required 10,000 ft apogee would require overcoming common hurdles associated with hybrid rocket engines, such as the lowered regression rates when compared to other liquid engines. Combatting these issues to ensure that the proper altitude is reached involved implementing several design modifications to a standard hybrid rocket motor. This paper focuses on the testing and

[1] Student, Mechanical, Aerospace, and Biomedical Engineering Department, AIAA Student.
[2] Student, Mechanical, Aerospace, and Biomedical Engineering Department, AIAA Student.
[3] Student, Mechanical, Aerospace, and Biomedical Engineering Department, AIAA Student.
[4] Student, Mechanical, Aerospace, and Biomedical Engineering Department, AIAA Student.
[5] Student, Mechanical, Aerospace, and Biomedical Engineering Department, AIAA Student.

implementation of three such design choices: the additively manufactured matrix-fuel grain, the nozzle with added post-combustion chamber, and the introduction of dissociative catalyst to the solid fuel. With these new design elements, the team hopes to see a marked improvement in the combustion efficiency, allowing the flight vehicle to reach the projected altitude with ease once implemented on the full-scale motor.

### A. Matrix Fuel Grain

Typical solid fuels used in conventional hybrid rockets utilize a solid fuel grain of some type of plastic, such as PVC or ABS, for its structural integrity. When introduced to the oxidizer, these solid fuels become extremely flammable, creating a combustion process which allows for the thrust necessary to propel the rocket. Contrary to standard grains, which are solid throughout, our design implements a matrix fuel grain which consists of hollow channels which run the length of the grain. Figure 1 below shows the difference between the matrix fuel grain and solid fuel grains by presenting the designs in a top-down view.

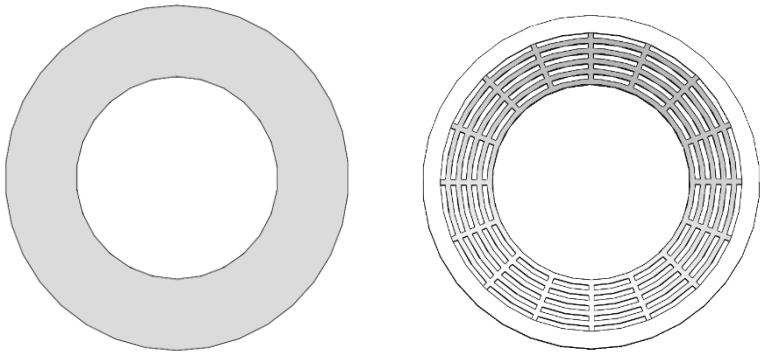

**Figure 1**. A top-down comparison of typical solid fuel grains (left) and the matrix fuel grain (right).

These channels are contained by thin walls of the structural element, in our case ABS plastic, and then filled with a powdered fuel type such as anthracite coal. Once the combustion has burned through the thin layer of plastic, it begins to ignite the powdered fuel which has a much higher regression rate due to its increased surface area. Once one layer of cells has been consumed, the process is repeated for the layers after, until the combustion reaches the thick outer wall and burns out, avoiding a burn-through of the grain. Addition of the cells and the higher-surface area fuel is expected to result in greater fuel regression, faster more complete burns, and a higher average thrust.

### B. Post-Combustion Chamber

Utilizing a powdered fuel in a matrix fuel grain exacerbates an issue that many other hybrid rocket designs have: not burning all of the fuel. When a cell in the matrix grain opens due to the burn-through of the cell wall, the powdered anthracite coal becomes exposed to the conditions within the combustion chamber. The coal is then burned in the combustion chamber, and the flow continues through the combustion chamber and out of the nozzle of the rocket. Most of the powdered coal is burned; however, a small portion does not burn up in the combustion chamber. Rather, it makes it through the nozzle throat without being used. This wasted coal lowers the efficiency of the rocket, as an ideal firing of the motor would burn all fuel before the flow exits the nozzle throat. Thus, a solution needed to be implemented.

A post-combustion chamber was determined to be the best solution for this problem. The post-combustion chamber is an open section past the fuel grain but before the converging section of the nozzle. This chamber allows for a circulation of the flow before it passes through the nozzle throat. This circulation of the flow provides more time for the coal to be burned, and this increase in fuel burned increases the overall efficiency of the motor.

The characteristic velocity, or C*, equation determines the combustion performance of a rocket motor. The significance of the C* equation is that it is independent of the rocket's nozzle performance. The equation for C* is shown below.

$$C^* = \frac{P*A_t}{\dot{m}} \tag{1}$$

This equation, however, is dependent upon the mass flow rate of the rocket. The mass flow rate is difficult to directly measure, so the mass of the fuel is measured before and after a flight. The pressure, however, can be directly

measured. Knowing the overall change in mass as well as the pressure over time within the combustion chamber, the equation can be rewritten as shown below [1].

$$C^* = \frac{A_t * \int P dt}{m_{burned}} \tag{2}$$

### C. Catalyst Introduction to Fuel

Hybrid rockets utilize an oxidizer mixed with solid fuel to maintain an exothermic reaction for propulsion. Nitrous oxide was used as an oxidizer due to its low cost and decrease in system complexity. The nitrous can be stored at a higher temperature as compared to liquid oxygen which requires more energy for cryogenic storage. Additionally, its self-pressurization properties allow for simplified thermal decomposition in reactive control systems and resistojets. However, due to its low density and resultant energy capacity, system efficiency must be carefully considered in low thrust applications [2].

Absolute efficiency implies complete dissociation of the nitrous oxide, yielding the maximum oxygen count supplied from the oxidizer. This also increases the probability of repeatable performance as the efficiency of the chemical reaction asymptotically approaches ideal dissociation. The nitrous oxide used has an activation energy of 250 kJ/mole which requires a temperature of 616.5 K for complete decomposition [3]. Such a high temperature allows for auto-decomposition since the breakdown of nitrous is exothermic, thus continuing the process. To decrease the activation energy of the nitrous, a catalyst can be implemented in the flow. Although there a multitude of compounds that act as catalysts, Roger Herdy at Qualis Corporation concludes that an array of metal-based catalyst beds can reduce the activation temperature of nitrous by up to 366.5 K [3]. These catalysts consist of transition metals embedded in minerals with microporous structures, known as zeolites, whose cations allow for transition metal anchoring. Once exchanged, the structure provides sieves that promote ion exchange between the chemically polar nitrous and catalyst, providing an attractive force on the oxygen [4]. Metal oxides also perform this interaction with a net positive charge that attracts the negatively charged dipole of oxygen ions in the nitrous. This supports the dissociation process by aiding in the net removal force on oxygen atoms, as opposed to solely relying on separation created from the momentum of molecules associated with kinetic energy in temperature [5].

### D. Test Stand Construction

When designing the rocket, there were a variety of different aspects that were changed. Instead of launching the rocket to test the impacts of such changes, a test stand can be used to measure the appropriate data. There are two types of thrust stands that can be used to measure the performance of a rocket motor. A horizontal stand, which has the rocket laying horizontal pushing against force transducer, and a vertical stand, which has the rocket pushing upwards against the force transducer, are the two types of test stands. In a horizontal stand, the effect of gravity will not be considered because the net thrust will be perpendicular to gravity. With a vertical stand, the weight of the rocket and restraints must be accounted for when calculating the total thrust of the rocket. Since the rocket is producing thrust parallel to the weight, there will be a time in which no net thrust will be produced. When using an oxidizer that is lighter than air, such as Nitrous Oxide, a vertical stand must be used. The pressure in the oxidizer tank forces the Nitrous Oxide to flow downwards, covering the entirety of the matrix fuel grain, in a vertical stance.

The main differences between the design of a horizontal and vertical stand is the restraint of the rocket within the stand. A vertical stand needs to provide a force that is equal or greater in amplitude than the net thrust that the rocket produces. One approach to provide such a force is by adding mass, and therefore weight, to the vertical stand. A large concrete pad can be used to add weight to the stand, while also providing a working surface. The concrete will need reinforcement to increase the tensile strength of the concrete. Additionally, a cap can be placed on the top of the stand. This cap acts as both a stop in the rocket escapes from its restraints and a place to put a force transducer. The cap will provide reinforcement against both shear and moment. The last approach to add mass to the stand is harnessing the rocket motor casing to an outside mass source. This source should act as a backup and will provide enough mass to ensure that the rocket cannot fly. Such a source can include a cubic meter tank of water place away from the stand. The rockets being tested produce approximately 600 pounds of thrust. If the rocket escapes its restraints, the ton of water will direct the rocket in arc towards the ground.

## III. Methodology

Before testing was done, the data acquisition equipment first had to be calibrated. This was done by placing barbell weights onto the S beam load cell one at a time. The weights used to calibrate were 3.24, 5.105, 5.130, 5.1375, 9.930, 9.950, 9.97, and 10.055 pounds. The load cell was connected to a breadboard and a Dataq DI1120, a data acquisition

instrument, that transferred a voltage from the load cell to a laptop. These voltages were collected using WinDaq, a data acquisition software that records voltages and displays them as a function of time on a graph. This data collected was then transferred from Windaq to another program, Tera Term, that converted the voltages to thrust data.

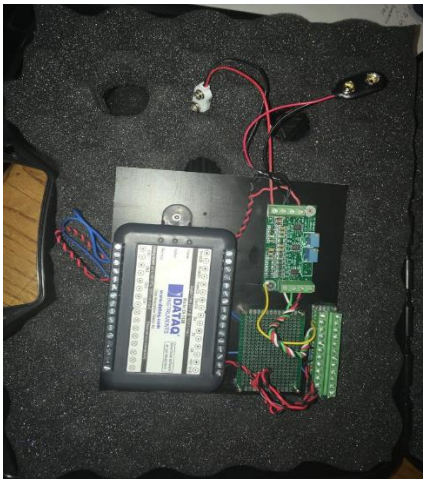


**Fig. 2** Data acquisition setup with Dataq DI1120 and breadboard

After the data acquisition device was calibrated, the motor housing was assembled. It consisted of an oxidizer tank on one end and a fuel grain matrix on the other. A pressure transducer was connected to the center of the motor housing to read chamber pressure after ignition. The igniter was then inserted into the bottom of the motor through the center of the fuel grain matrix. This igniter consisted of an E-match, a black powder charge, and a fill line for the oxidizer. Once assembled, the motor casing was attached to the small-scale test stand with hose clamps and the load cell was fastened to the top.

Using the fill line inserted into the motor casing, the oxidizer tank was filled with nitrous oxide until a white cloud could be seen exiting an exhaust tube. This signaled that the oxidizer tank was full. The ignition switch was then flipped, sending a current through the E-match igniting the black powder charge. This charge burned through the fill tube, stopping the flow of nitrous oxide and igniting the engine.

## IV. Results and Discussion

### A. Matrix Fuel Grain

The matrix fuel grain implementation was one of the first design choices we tested, with testing occurring in early December of 2018. The testing was performed using one solid fuel ABS grain, a PBAN grain with 10% Al added in a matrix-like configuration to mimic the matrix fuel grain design, and then a matrix fuel grain with added anthracite coal. The thrust data was then collected and compared below in Fig. 3.

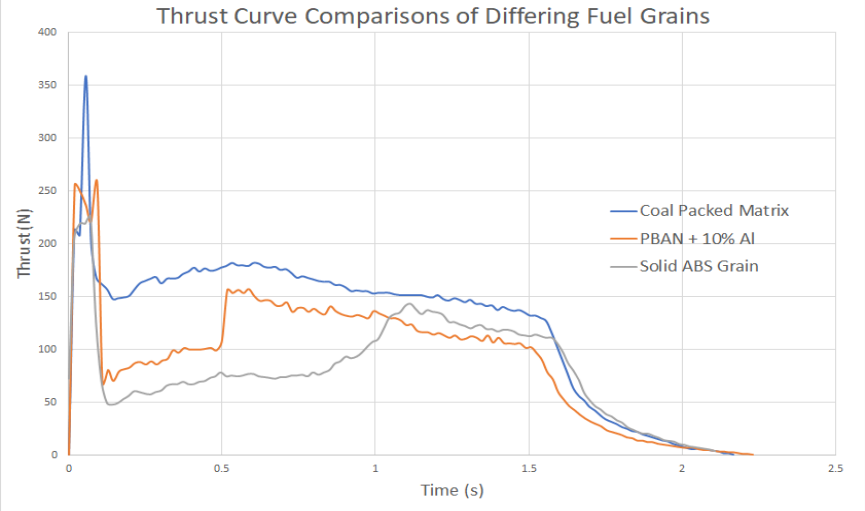


**Fig. 3** Thrust curve comparisons of differing fuel grains.

As expected, the coal-packed matrix performs the best when compared to conventional fuel types, with higher peak and average thrust. Also exemplified in the graph is the shorter ignition time present in the matrix fuel grain, allowing for a larger amount of energy to be added to the fluid flow over the course of the burn.

To better quantify the increased performance from these contributions, the grains were weighed before and after firing. The tank of nitrous was also kept at a constant temperature to assure the same density throughout the firings, resulting in the same amount of oxidizer being consumed for each firing. These values were checked by the thermophysical property code for nitrous oxide. Once the mass expended was determined, total impulse was then calculated via Eq. (3).

$$I_{tot} = \int_0^{t_{burn}} T(t)dt \tag{3}$$

With the total mass consumed during the burn, assuming mass lost by the grains was in fact completely consumed during the combustion, and the total impulse $I_{tot}$, we could then calculate specific impulse using Eq. (4).

$$I_{sp} = \frac{I_{tot}}{\dot{m}g_0} \tag{4}$$

Specific impulse allows us to compare the relative efficiencies of the burns by returning a comparable value which is not dependent on the mass burned. The specific impulse increase from 94.6 for the standard ABS grain and 113.2 s for the PBAN with 10% Al grain, to 144.2 s for the coal-packed matrix, proves our hypothesis correct that the grain design would boost combustion efficiency and provide better performance overall.

In further tests of the matrix-grain design, a fuel-rich exhaust was noticed consistently at each firing. This was theorized to be the result of the packed coal being released from the cells once the burn began and pushed out of the motor before it could fully ignite, resulting in coal ignition outside of the motor. To counteract this, future tests would include a post combustion chamber which would create extra length before the nozzle throat, allowing time for the coal to ignite and combust more completely.

Another issue observed through testing was compacting of the coal powder through capillary packing methods. Capillary packing involves filling the cells with coal and then dropping the matrix grain from a consistent height. When the grain hits the surface, the coal, still moving, is pushed further down into the grain. While this allowed us to contain more anthracite coal within the matrix, the problem is that the capillary packing caused the powdered coal to begin compacting upon itself. Once compacted, the powder loses the benefit of having a higher surface area which makes it harder to completely burn. This was fixed implementing a mechanical coal sifter which vibrates from the middle of the grain, agitating the coal within the cells, causing them to completely fill the lengths of the cells without compacting upon each other. These design implementations will be utilized for the full-scale grains and tested before the full-scale launches in mid-May and early June.

### B. Post-Combustion Chamber

Two separate motor tests were performed. One test utilized the post-combustion chamber whereas the other did not. The test without the post-combustion chamber was performed with only thrust measurements taken, and the test

with the post-combustion chamber only had pressure measurements taken. In order to compare the results of these two tests, the pressure data must be converted to thrust, and the thrust data must be converted to pressure. The two equations below convert these values, with Eq. (5) converting pressure to thrust and Eq. (6) converting thrust to pressure [6].

$$T = C_N * A_t * P \tag{5}$$

$$P = \frac{T}{C_N * A_t} \tag{6}$$

The nozzle coefficient used in the above equations was 1.4. The diameter of the nozzle's throat was measured to be 0.375in, which meant the area of the throat was 0.11045in$^2$. The units for the above equations would result in pounds per square inch for pressure and pounds for thrust. These output values were then converted into Pascals and Newtons.

The measured thrust data for the test without the post-combustion chamber and the calculated thrust data for the test with the post-combustion chamber is shown below. Also, the thrust curves of tests with varying C* values are shown as well.

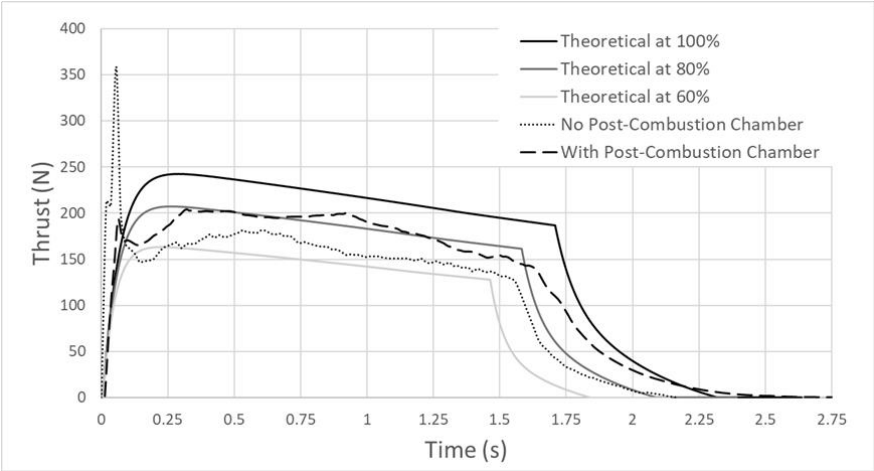


**Fig. 4** Thrust vs. Time for two real tests and three theoretical tests at various C* values

The theoretical thrust values were calculated using a Matlab code that accurately models the characteristics of the motor during test fires. The "ideal" fire represents having just enough oxidizer to burn all of the fuel within the grain. With the mass of fuel grain being 48.4 ± 0.1 g, the exact amount of oxidizer necessary for complete combustion is 0.168 kg of $N_2O$. This corresponds to a temperature needed within the nitrous chamber of 286K.

Each theoretical line in the figure above represents the thrust curve at different C* values. The 100% line is an ideal test fire where all fuel is burned, and the other two theoretical lines have C* values at 80% and 60% of the ideal version. The ideal C* of the motor tested is 1730.3m/s, or 5676.8ft/s. The C* for the 80% theoretical test is 1384.2m/s, or 4541.3ft/s, and the C* of the 60% theoretical test is 1038.2m/s, or 3406.2ft/s.

As stated previously, the test without the post combustion chamber had thrust directly measured, whereas the thrust for the test with the with the post combustion chamber was calculated from the pressure. The thrust for the theoretical tests was also calculated using the above equation relating the pressure to the thrust. That is why the only test shown in Fig. 4 above with a high peak value is the test where the thrust was directly measured. The pressure within the combustion chamber of the motor does not exhibit a peak like the thrust doe, so the calculated thrust values do not show peak values.

Figure 4 above shows that test without the post-combustion chamber hovers around the high 60% C* value, and the test with the post-combustion chamber follows the 80% C* line. This figure shows an overall improvement in the thrust produced by the motor by utilizing a post-combustion chamber. However, the peak thrust values of the two tests cannot be compared. The peak thrust values indicate the ignition characteristics of the motor, and while the converted pressure does have a slight peak, the spike in the thrust of the test with the post-combustion does not compare to the peak in the thrust of the other real test in Fig. 4.

To calculate C* values of the two tests, the pressure data is needed. The theoretical pressure values as well as the measured and calculated pressure data from the two tests are shown below in Fig. 5.

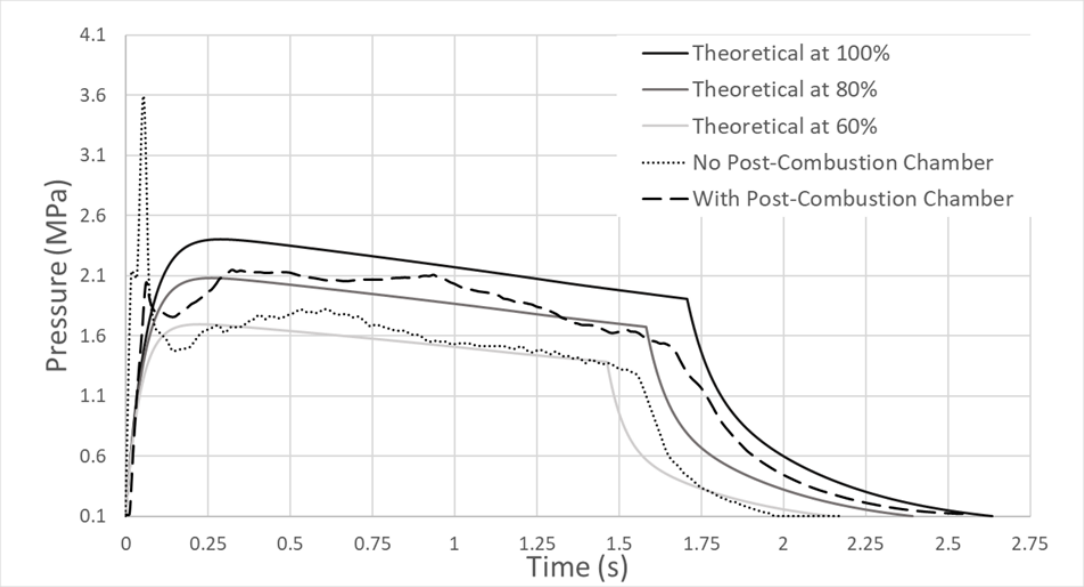


**Fig. 5** Pressure vs. Time for two real tests and three theoretical tests at various C* values

Figure 5 above shows the same lines as the graph in Fig. 4. In this graph, the test using the post-combustion chamber had the pressure measured outright whereas the non-post-combustion chamber test's pressure was calculated from the thrust. The line for the test with the post-combustion chamber again hovers around the 80% efficiency line, and the line for the test without the post-combustion chamber stays near the 60%.

Using the pressure data shown above, the C* for both real tests was calculated. The C* for the test without the post-combustion chamber was calculated to be 1159.3m/s, or 3083.5ft/s. The test with the post-combustion chamber was 1488.1m/s, or 4882.2ft/s. This equates to a 67% and an 86% efficiency values for the non-post-combustion chamber and with post-combustion chamber tests, respectively. Thus, the addition of the post-combustion chamber to the motor increased the efficiency of the combustion by 19%, and the overall efficiency is much closer to ideal.

The peak in the pressure data for the test without the post-combustion chamber is due to it being calculated from the thrust. As the thrust has a peak value near the beginning of the test when the ignition process occurs, the calculated pressure values follow suit. However, as shown from the test where pressure was measured outright, there is no peak in the pressure values. This could have caused an issue in the calculation of C* for the test without the post-combustion chamber as the peak might have increased the overall C*.

In order to improve the accuracy of these results, both thrust and pressure measurements need to be taken during all test fires. While the pressure data can be converted into thrust and vice versa, the results would be much more reliable if the thrust was measured outright. More tests should be performed with each nozzle, so the family of data can be compared. In this way, an overall view of the two versions of the chambers, one with the post-combustion chamber and one without, can be compared.

### C. Catalyst Introduction to Fuel

Nickel (II) oxide was the catalyst selected in this experiment due to its low cost and accessibility. For even comparison between catalyst implementation and base design performance, the overall system was unchanged. This was done by homogeneously mixing the catalyst with anthracite coal and packing into the existing solid fuel grain design. Grain A contained 7.809 g pure anthracite coal. Grain B consisted of anthracite coal and 1.014% catalyst by mass. The coal and catalyst had total masses of 7.529 g and 0.077 g respectively yielding a solid fuel mass of 7.606 g. The mass of nitrous used in test A and B was measured to be 0.131 kg and 0.129 kg respectively. Based on nitrous properties, its temperature was calculated using the defined volume of the chamber which yielded a condition of 306 K for tests A and B. The ideal pressure curve was found using propulsion analysis software assuming complete combustion of solid fuel and its required oxidizer count. This requires a temperature of 286 K corresponding to 0.169 kg of nitrous contained within the initial chamber. The characteristic velocity was used to quantify the performance in each test. The ideal process yields a C* of 1730 m/s which was used in comparison to grains A and B with 520 m/s and 1020 m/s accordingly. Figure 6 graphs the compared combustion processes between each grain along with a base analysis of ideal combustion characteristics.

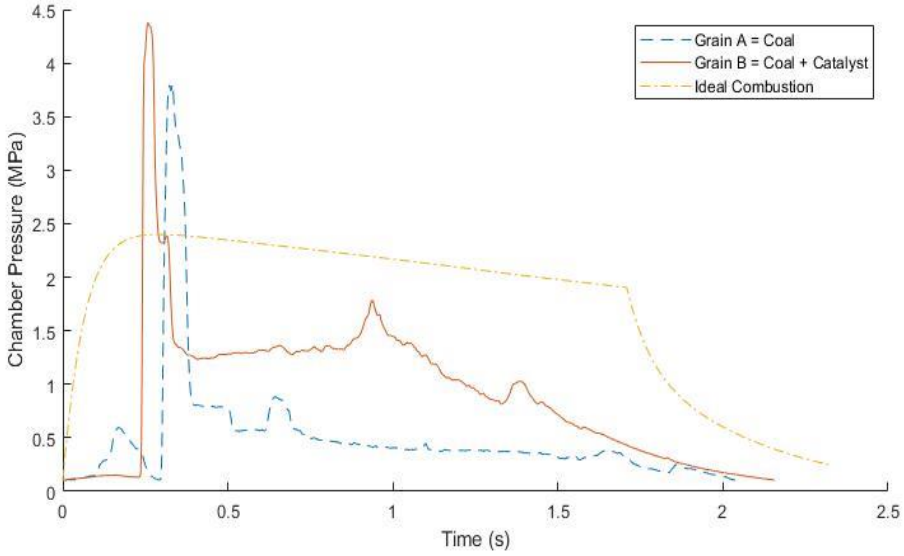


**Fig. 6** A comparison of the combustion chamber pressures during ignition between implemented catalyst and standard coal fuel grains. An ideal combustion pressure process is also shown as the desired standard.

The conducted experiment provided strong preliminary results before and after a catalyst implementation. Both grains underperformed as compared to ideal, indicating partial combustion. This is due to the high nitrous temperature of 306 K that occurred during both tests. The nitrous oxide experiences a critical temperature of 308 K under atmospheric conditions; thus, the oxidizer was exceedingly transitioned into its gas phase. This lowers its density and as a result, its oxygen count and vapor pressure. Additionally, the lower nitrous flow may not yield sufficient oxidizer to ignite the solid fuel which is needed for perpetual ignition. Because the system is oxygen starved in both tests, the catalyst grain shows notably better performance because of its ability to provide oxygen dissociation at lower temperatures. The solid fuel with catalyst performed a characteristic velocity of 1020 m/s whereas the pure coal grain produced a C* of 520 m/s under similar conditions. It must be noted that the peak pressures created in grain A and B analysis are likely due to ignition system and pressure transducer errors.

### D. Test Stand Construction

The vertical test stand design starts at the pad and frame. For this test stand, the frame consisted of a single 4-inch by 10-foot I-beam. The I-beam had a steel plate welded to the bottom, with a 4 by 4 foot, 16-inch deep concrete pad poured around the beam. The steel plate provided a larger amount of surface area for the concrete to interact with. Additionally, the concrete had glass strands placed in the mixture to increase the tensile strength. A 4-inch square half inch thick tube was used as the cap for the stand. This 2-foot long section of tube was placed in the I-beam to oppose any shear and moment the rocket produced. To oppose the shear, the tub would slide around the I-beam. This was done by slotting the tube and slitting the I-beam such that the tube would slide around the I-beam. Additionally, a 3-quarter inch bolt was placed perpendicular to the slot to ensure the tube would compress and grab onto the beam. Two steel triangles were place on the top front of the tube to oppose any moment that the rocket produced. These triangles were welded to the tube such that the vertical face of the triangle would push against the beam. Additionally, two metal clamps were used on the backside of the tube to completely harness the tube into place around the beam. A slit was added to the tube to allow a force transducer to be moved forwards and backwards. This was done to allow for different size motors to be tested without having to change the cap.

The next part of the test stand was the rocket mount. Since the beam only had a thickness of 4 inches, a plate was required to attack a set of rails that the motor mount was attached to. This 2 by 5-foot plate would be attached to the I-beam through the use of 10 rows of 2, half inch bolts. The rails were mounted in a similar fashion but further from the vertical center line of the plate. Additionally, these rails only used 20, quarter inch thick bolts. The motor mount used in this vertical test stand consisted of four linear bearings and another 4-inch square tube. The linear bearings create a mount that can slide up and down to allow for different sized motors to be used in the stand. The motor was restrained within the tube using two U-bolts to clamp the casing to the mount. Also, a smaller U-bolt is bolted to the tube to provide a location to tether the motor to the water tank.

**Fig. 7** This figure shows the completed vertical test stand.

With this vertical test stand, the main concern is the safety for those who are testing the rocket. To increase the factor of safety, an implementation of multiple safety factors is included. The first is that the motor is properly secured to the mount and firmly pressed against the force transducer. However, if the any of the bolts shear, a 'unzipping' effect might occur. In the case this situation occurs, the cap will be a secondary safety factor. The cap was designed to oppose any shear and moment the motor creates. By over designing the cap, any unwanted motion of the rocket motor should be hindered. Finally, the last safety factor is the tether. If the motor escapes, the tether will guide the projectile into the ground. Since any motion of the rocket would be unpredictable, the tether would ensure that the rocket would not fly around and endanger anyone around the test stand area.

Although the vertical test stand was built, there are a few things that should be done to ensure the maximum amount of safety and reducing the amount of setup for future groups. The first and biggest issue is that the beam is a fixed-free beam. Since the beam is only connected at the ground, the top is free to move around. The concern is that rocket might oscillate the top of the beam, creating a hazardous testing environment. There are several solutions to this problem that could be implemented in the future. The first is bolting another beam to the I-beam. This secondary beam would increase the amount of material to counteract any motion the original I-beam may produce. Another idea is to use the system that telephone poles use to stabilize the free end of the pole. Two cable would be attached to the top of the I-beam and to mounts that are placed in the ground or the concrete. These cables would act as restraint for the top of the I-beam and only extend out to the edge of the concrete pad. The other issue that needs to be approached is ensuring that the motor mount will not slide from the rails and will be locked into place during testing. There are number of potential solutions to this issue such as using clamps on the rails that act as stoppers for the linear bearings. Another solution includes bolting brackets at the appropriate height.

## V. Conclusion

As the project continues, the results of these motor implementations will allow us to increase the combustion efficiency of the full-scale motor as well as implement even more design changes for better performance. Exploring more catalyst options through continued subscale testing is certainly possible due to the results of the previous firings and the relative ease with which catalysts are added to the fuel. Changing igniter systems from Pyrodex to thermite ignition, as well as flammable paint to coat the interior of the grains, are some other design elements which will be tested and analyzed as the competition date draws nearer. Construction of the vertical test stand and the acquisition of the full-scale motor allows the design team to begin hydro-testing and static firing the motor by early May, with scheduled full-scale launches occurring in mid-May and early June. With the experimental nature of both the payload and the motor itself, the Spaceport America Team expects to place exceptionally well in the competition, and hopes to take the lessons learned and discoveries made during this year's design phase and carry on for next year's entrance to the 30,000 ft. altitude category.

## References


[1] Nakka, R., "Solid Rocket Motor Theory -- Impulse and C-Star," *Richard Nakka's Experimental Rocketry Web Site*, 2001, [online website] URL: https://www.nakka-rocketry.net/th_imp.html [Accessed May 3, 2019]

[2] Palacz, T. (2017) AGH Space Systems, Nitrous Oxide Applications for Low-Thrust and Low-Cost Liquid Rocket Engine. (n.d.). Retrieved May 1, 2019, from https://www.researchgate.net/publication/318274912_Nitrous_Oxide_Application_for_Low-Thrust_and_Low-Cost_Liquid_Rocket_Engine

[3] Herdy, R. (2001) Qualis Corporation, Nitrous Oxide / Hydrocarbon Fuel Advanced Chemical Propulsions: DARPA Contract Overview. (n.d.). Retrieved May 1, 2019, from (https://tfaws.nasa.gov/TFAWS06/Proceedings/Aerothermal-Propulsion/Papers/TFAWS06-1026_Paper_Herdy.pdf

[4] Naccache C., Taarit B., Transition Metal Exchanged Zeolites: Physical and Catalytic Properties. (1984). Retrieved May 2, 2019, from https://link.springer.com/content/pdf/10.1007%2F978-94-009-6128-9_14.pdf

[5] Cengel Y., Boles M., Thermodynamics, 8th ed., McGraw-Hill Education., 2015

[6] Nakka, R., "Solid Rocket Motor Theory -- Thrust," *Richard Nakka's Experimental Rocketry Web Site*, 2016, [online website] URL: https://www.nakka-rocketry.net/th_thrst.html [Accessed May 3, 2019]